

The effect of polar (111)-oriented SrTiO₃ on initial perovskite growth

Ingrid Hallsteinsen¹, Magnus Nord², Torstein Bolstad¹, Per-Erik Vullum^{2,3}, Jos E. Boschker^{1,a}, Paulo Longo⁵, Ryota Takahashi⁴, Randi Holmestad², Mikk Lippmaa⁴, and Thomas Tybell^{1,b}

¹ Department of Electronics and Telecommunications, Norwegian University of Science and Technology (NTNU), Trondheim, 7491, Norway

² Department of Physics, Norwegian University of Science and Technology (NTNU), Trondheim, 7491, Norway

³ SINTEF Materials and Chemistry, 7456 Trondheim, Norway

⁴ Institute for Solid State Physics, University of Tokyo, Chiba 277-8581, Japan

⁵ Gatan Inc., 5794 W Las Positas Blvd, Pleasanton CA, 94588, USA

In crystalline thin film growth of a prerequisite is substrate surfaces with stable and uniform structure and chemical composition. Various substrate treatments were used to obtain

^a Present address: Paul-Drude-Institut für Festkörperelektronik, Hausvogteiplatz 5-7, 10117 Berlin, Germany

^b Corresponding author: thomas.tybell@iet.ntnu.no

atomically smooth, step-and-terrace (111)-oriented SrTiO₃ with uniform cation layers at the surface, i.e single termination. The surface control enables subsequent layer-by-layer epitaxial growth of perovskite thin films of La_{0.7}Sr_{0.3}MnO₃, LaFeO₃, and BaTiO₃. Reflection high-energy electron diffraction and electron energy loss spectroscopy revealed that a single chemically intermixed (A,A')BO₃ perovskite layer formed at the interface. As the terminating layer of (111) SrTiO₃ is polar, a surface reconstruction consisting of TiO_x surface layers is expected, and the intermixing at the interface can be understood as A'-cations from the film material compensating an A-cation deficient substrate surface during initial growth. This finding has important consequences for engineered interfaces between perovskite thin films and polar substrate facets.

The development of atomically well-defined substrate surfaces is a major driving force behind controlled epitaxial growth and recent advances in complex oxide thin film synthesis.¹ As complex oxides exhibit strong structure-property coupling, epitaxy can be used to control the functionality of the film, utilizing strain or crystalline orientation. Different orientations of a substrate will result in interfaces where symmetry, surface polarity, and octahedral coupling differ, possibly affecting the electronic states of the epitaxial film at the interface. To exploit such effects, substrates of stoichiometric crystals with atomically flat surfaces of single termination and without major reconstructions are required.²⁻³ SrTiO₃ (STO) and different rare-earth scandates have been widely used as substrate materials for perovskite thin film growth due to the good lattice match with materials of interest and chemical stability. The surfaces of these materials have been extensively studied since the 1990s, and high-quality (001)-oriented substrates are commercially available.⁴⁻⁶ However, for (111)-oriented STO, well-defined single-terminated stoichiometric surfaces have been more difficult to obtain due to the polarity of the terminating surface.^{3, 7}

A schematic of the (111)-oriented STO surface is depicted in side and plane views in figures 1a and b, respectively, where Ti is colored yellow, Sr blue and O turquoise. The (111)-surface has a hexagonal symmetry, where the low-index in-plane crystallographic directions $[10\bar{1}]$ and $[11\bar{2}]$ are indicated in figure 1b. Along the $[111]$ -direction STO consist of alternating layers of SrO₃⁴⁻ and Ti⁴⁺, which are each stacked in a “ABCABC...” manner as marked for the Ti⁴⁺ layers in figure 1a and b. The distance between two equally terminated planes is $d_{111} = a/\sqrt{3} = 2.25\text{\AA}$ (figure 1a), where a represents the cubic lattice constant of STO ($a = 3.905\text{\AA}$). Ideally, single terminated STO(111) would solely have SrO₃⁴⁻ or Ti⁴⁺ as the uppermost layer, in the schematic a Ti-terminated layer is shown. Hence, STO(111) has layers of nominal charge +4/-4, whilst STO in the (001) orientation consists of layers of SrO and

TiO₂ and is thus non-polar. Since the surface energy of an ideal polar surface diverges,⁸ polar surfaces tend to facet or form stabilizing reconstructions. This makes film growth on a STO(111) substrate more challenging than on non-polar STO(001), with a tendency to form a disordered interface.⁹⁻¹¹ We have earlier shown that by reducing the deposition temperature, it is possible to delay the onset of surface roughening, allowing for smooth surfaces in a certain thickness range.¹² Still, several reports point towards new phases and different reconstructions at the interface between a substrate and a (111)-oriented film.^{7, 13}

Substrates having uniform single terminations are necessary for obtaining structurally stable interfaces with a film material.¹⁴ For (001)-oriented STO, a uniform TiO₂ termination can be achieved by selective wet etching in buffered hydrogen fluoride, which preferentially removes SrO from the surface.⁴ For (111)-oriented STO there are several reported surface preparation methods pointing towards the possibility of having a stable single termination. For instance, annealing in a reducing atmosphere has been reported to give single terminated surfaces.¹⁵ However, high-temperature treatment in a reducing atmosphere can result in oxygen deficiency, resulting in metallic conductivity and even ferromagnetic behavior.¹⁶ Annealing in O₂-atmosphere and chemically etching with HCl:HNO₃ give a step-and-terrace surface structure with steps corresponding to 1/2 monolayer, indicating that the terminating layer alternates between the SrO₃ and Ti layers on adjacent terraces.¹⁷ Several authors have reported single monolayer step-and-terrace structure for STO(111) by combining buffered hydrogen fluoride etching with high-temperature annealing in O₂ atmosphere.¹⁸⁻¹⁹ As SrO₃⁴ reacts with water to form Sr(OH)₂, while Ti⁺⁴ is not water-soluble, an almost identical result was reported by using deionized water as the etching reactant,^{18, 20} however the use of buffered hydrogen fluoride results in a more complete removal of Sr-related compounds.¹⁸

Here we present a study of how the polar surface of STO(111) influences the initial thin film growth. We discuss the effect of substrate preparation on thin film synthesis, and how possible reconstructions affect the stoichiometry of the thin film/substrate interface, important for interface engineering of (111)-oriented thin films.

Experimental:

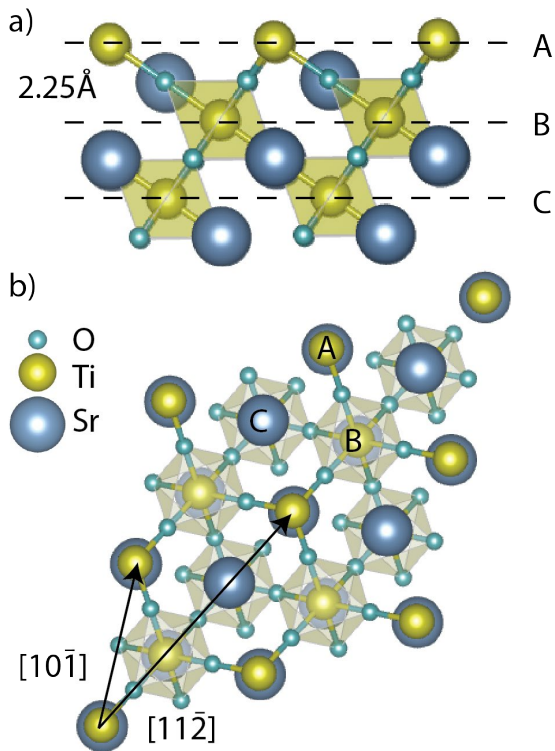
Two different treatments of the (111)-oriented STO substrates (Shinkosha, $10 \times 10 \text{ mm}^2$) are compared in this study, where deionized-water and buffered hydrofluoric acid are used as etching agents. Both etching chemicals have been reported to produce atomically smooth surfaces with a single terminating layer.¹⁸ For both methods the substrates were cleaned prior to etching in acetone and ethanol for five minutes under ultrasonic agitation. Annealing was done under oxygen flow after the etching process with a ramp rate of 5K/min. The first treatment method (DI) consists of immersing the substrates in 80 mL of deionized water at 70°C under high-temperature ultrasonic agitation for 30 min before annealing at 1200°C for 2 hours. In the second treatment method (BHF), the substrates were immersed in deionized water at 70°C and held under ultrasonic agitation for 5min, before dipped in buffered hydrofluoric acid for 45s and rinsed in deionized water, ending with an annealing at 1050°C for 1 hour. The buffered hydrofluoric acid solution was $\text{NH}_4\text{F}:\text{HF}$ 7:1, with a pH of 4.7. The annealing times and temperatures were chosen after optimization based on atomic force microscopy (AFM) investigations.

Ultrathin films of $\text{La}_{0.7}\text{Sr}_{0.3}\text{MnO}_3$ (LSMO), LaFeO_3 (LFO), and BaTiO_3 (BTO) were deposited by pulsed laser deposition at 520-580°C in 0.35 mbar (0.01 mbar for BTO) of oxygen ambient with a KrF excimer laser (248 nm) at a fluence of $\sim 2 \text{ Jcm}^{-2}$ and a repetition rate of 1 Hz. The substrate to target distance was 45 mm. After deposition the films were cooled to room temperature in 100 mbar of oxygen at a rate of 15 K/min. Reflection high

energy electron diffraction (RHEED) was used to monitor the growth in-situ. AFM (Veeco Nanoscope V) was used to study the surface topography. Friction force microscopy (FFM) with a cantilever spring constant of 0.9N/m was used to study the termination of the substrates. Coaxial impact-collision ion scattering spectroscopy (CAICISS) was used to investigate the chemical composition of the substrate surface. Scanning transmission electron microscopy (STEM) data were obtained on a double-corrected Jeol ARM200CF microscope equipped with a Gatan Quantum ER for electron energy loss spectroscopy (EELS). Cross section TEM lamellas were prepared by a FEI Helios Nanolab Dual-Beam Focused Ion Beam (FIB) using standard lift-out technique. All STEM- high angle annular dark field (HAADF) data were acquired at collection semi-angles of 73-311 mrad, and for all EELS data an energy dispersion of 0.5 eV/channel and a collection semi-angle of 66 mrad were used. All EELS analysis was performed using HyperSpy.²¹

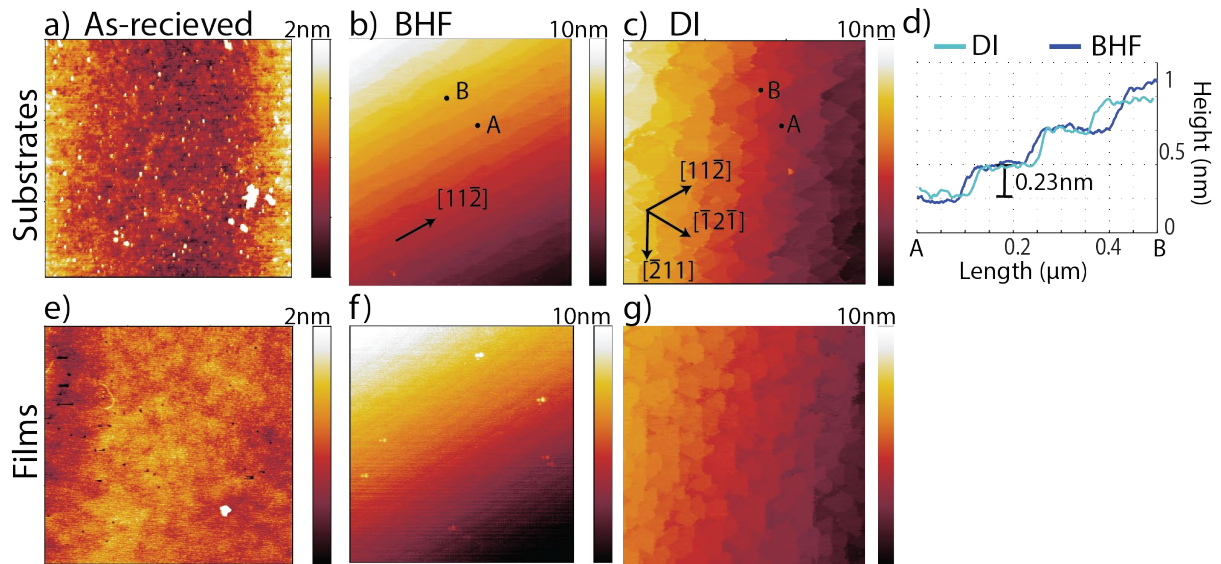
Results:

An AFM image of an as-received substrate is shown in figure 2a, revealing a relatively flat surface with a root mean square roughness of 0.36 nm. The surface is disordered with structures of multiples of half d_{111} , indicating mixed termination. Figure 2b and c show substrate morphologies after annealing, which were pretreated with the BHF and DI methods, respectively. In both cases, ordered surfaces were obtained with a clear step-and-terrace structure. In figure 2d AFM line scan profiles are shown for both BHF and DI treated substrates, revealing that both methods result locally in step-heights of 0.23nm and flat terraces of 100-150 nm width, in agreement with the substrate miscut angle of 0.1° . The measured step height correspond to STO d_{111} , indicating that all terraces are terminated by identical atomic layers in accordance with the findings of Chang et al.¹⁸



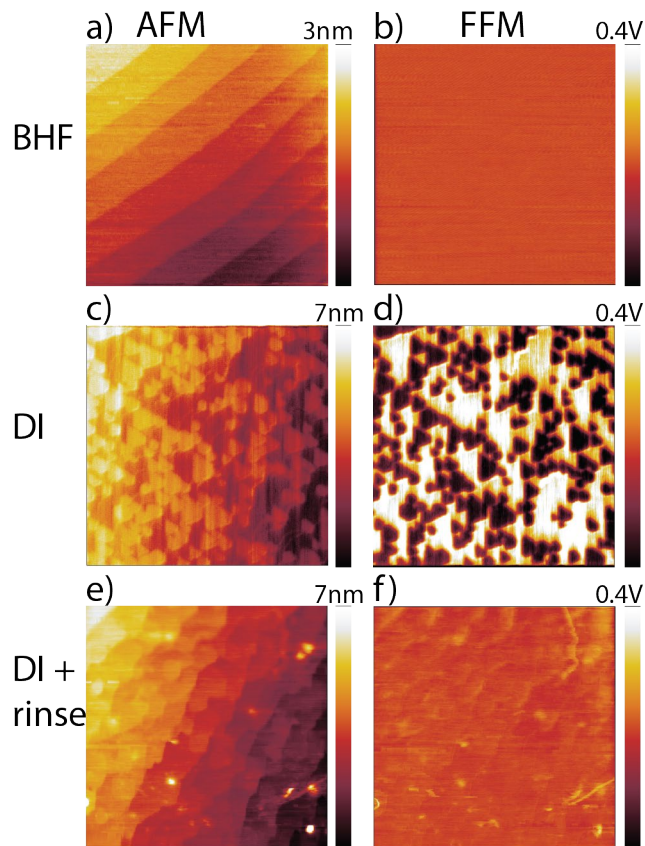
A morphological difference is observed between substrates prepared with BHF and DI methods. The substrates pretreated with BHF (figure 2b) reveal steps and terraces that are straight. However substrates pretreated with DI, as in figure 2c, have faceted step edges forming triangular sections. The step edges make a zig-zag pattern, where the direction of the edge changes by 60° or 120°. Based on the crystal orientation of the substrate, the step edges tend to follow the crystallographic axes, as indicated in figures 2b and 2c. For the BHF substrates the step edges are parallel to one of the three $\langle 11\bar{2} \rangle$ in-plane directions in accordance with the miscut direction. This is also the case for the DI substrates, except that the step edges in this case make the zig-zag pattern along all three $\langle 11\bar{2} \rangle$ in-plane directions. We note that for STO(001) such faceted step edges have earlier been reported for Sr-rich terminations.¹ The morphologies of LSMO films of approximately 10nm grown on as-received, BHF and DI substrates are compared in figure 2e-g. The morphologies of the films replicate the substrate surfaces accurately, which means that the substrate surface is stable at

the deposition temperature (500-600 °C) and acts as a mold for the film as long as the film grow layer by layer.¹²



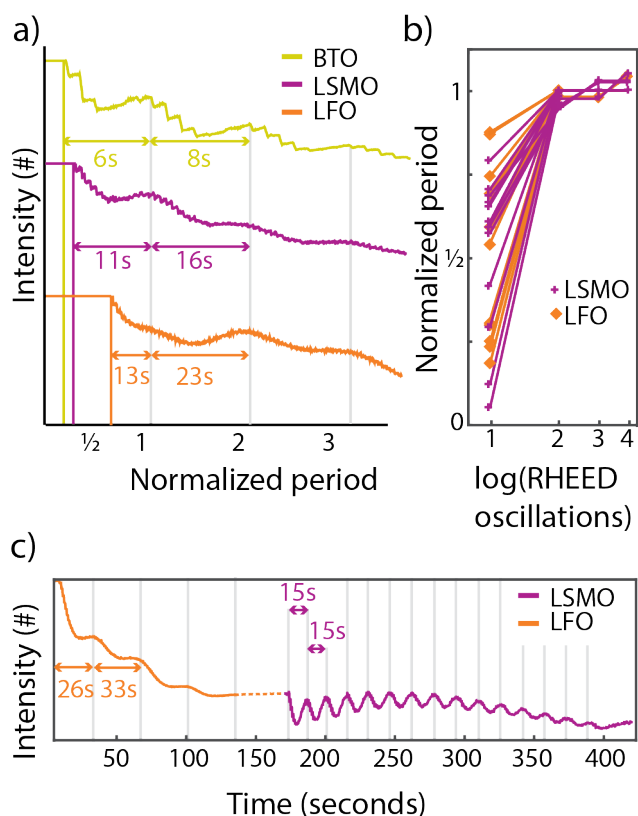
To further investigate the termination and chemical composition of the substrates, friction force microscopy (FFM) was used. In figure 3 we show the contact-mode topography and friction contrast for BHF (a, b) and DI (c, d) prepared substrate surfaces. For BHF substrates no significant friction contrast is observed, indicating no macroscopic chemical composition contrast on the surface. For the DI case, there is friction contrast visible, with two distinct levels compatible with areas of different cations. Comparing topography and friction data, it is a clear that the faceted terraces are split into triangles of different friction contrast. Based on comparison with FFM measurements of SrTiO₃ (001) surfaces, the dark contrast are inferred to be Sr-rich areas and the bright contrast Ti-rich areas.²² AFM analysis also reveals that Sr-rich regions are rougher than the Ti-rich terraces, and that they lie approximately 1/2 and 3/2 d_{111} above the Ti-rich terraces.

One possible way for the substrate to stabilize the polar surface is by forming non-stoichiometric surface reconstructions.^{3, 24} Different substrate pretreatments have shown a variety of surface reconstructions on (111)-oriented STO,²⁵⁻²⁸ where the polarity is screened by surface TiO_x layers. Angle-resolved CAICISS measurements were performed on DI and BHF treated substrates to test the chemical composition of the substrates. The time-of-flight surface composition analysis revealed increased presence of Sr on both DI and BHF prepared substrates as compared to as-received (see supporting information), suggesting the occurrence of Sr segregation during annealing. We note that the longer annealing time and higher annealing temperature for the DI (2 h, 1200°C) compared to the BHF (1 h, 1050°C) may lead to segregation of Sr,²³ and the reason for the difference in FFM. To test if the Sr signal corresponds to segregated atomic Sr on the surface, we rinsed the DI substrate with DI-water 70°C for 2 min in ultrasonic bath, followed by 5 min on a hot plate of 100°C to evaporate all the remaining liquids. The results shown in figure 3e and f reveal that the faceted step-and-terrace structure is still present, however the FFM data now gave a homogeneous contrast. We interpret this as atomic Sr being removed from Sr-rich areas, resulting in a single termination state.

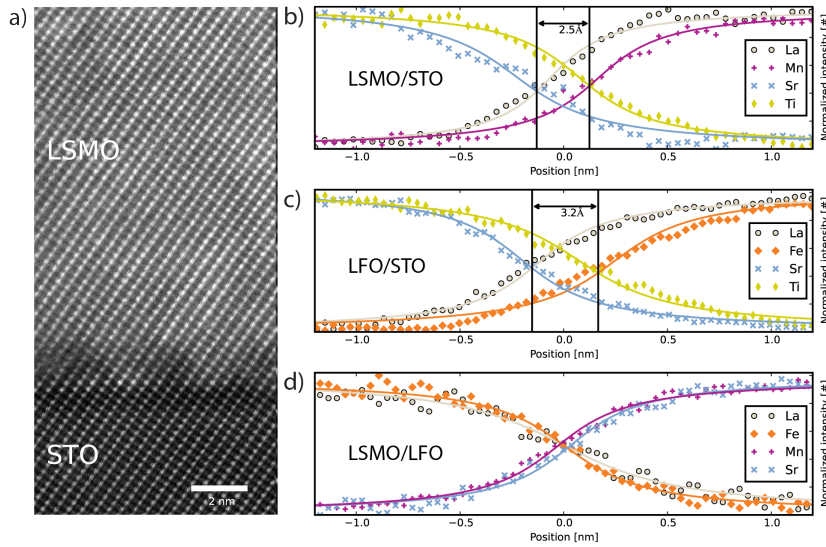


In thin film epitaxy, the ad-atom mobility and possible growth mode depend on the chemical environment of the underlying layer.¹ Hence the growth of the first unit cell of a thin film on top of the substrate may indirectly identify the chemical environment of the substrate. Using substrates prepared by the BHF method and recording the intensity oscillations of the RHEED diffraction spots we investigate the growth of the first unit cells of a thin film. In figure 4a RHEED oscillations for different film materials are plotted. The maximum of each oscillation is taken as a complete layer, consistent with the longest intensity recovery time for each pulse indicating no phase shift.²⁹ For clarity the signals have been normalized to the growth period (number of laser pulses per RHEED oscillation) of each film material. As can be seen in figure 4a, the growth period remains constant throughout the growth of the film except for the first complete layer. It is clear that for all three materials investigated here, the first RHEED oscillation is shorter than the growth period for the subsequent layers. In figure

4b statistics for the first oscillation normalized to the growth period is shown, and the first layer has typically a growth period of 30 – 90% as compared to the subsequent layers. Hence, the amount of pulses needed to synthesize the first layer varies from film to film, but is observed to always be shorter than the growth period of the subsequent layers independent of film material or deposition parameters. Moreover, the growth period for the first layer is not consistent with half a period, which would indicate a change of termination, as observed for SrRuO₃ growth.³⁰⁻³¹ In figure 4c a RHEED intensity plot for an LSMO/LFO/STO(111) epilayer is shown. It is clear that for the first LFO layer the corresponding RHEED oscillation has a shorter period (26s) as compared to the subsequent layers (33s). However, for the top LSMO film the first RHEED oscillation has the same period as for the subsequent layers, measured at 15s for this particular sample. Hence we interpret that the shorter growth period at the substrate/thin film interface is an effect due to the substrate surface.

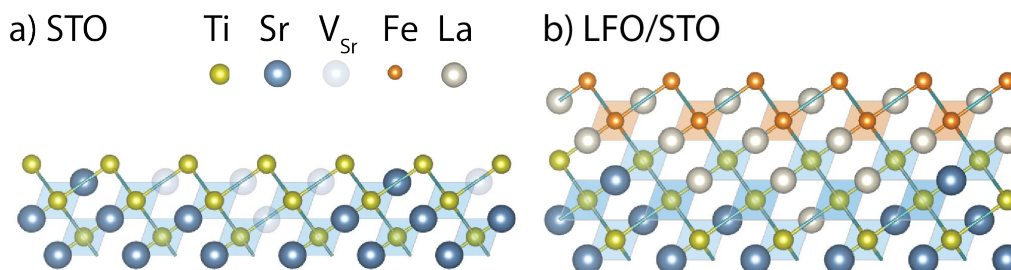


To further investigate the chemical interface between substrate and thin film, STEM and EELS investigations were performed across the substrate-film interface. The STEM data in figure 5a indicate that the film is epitaxial, fully strained and of high crystalline quality. Cross section composition analysis of the interface regions was obtained from EELS measurements across the LSMO/STO(111) and LFO/STO(111) interfaces, and is shown in figures 5b and 5c respectively. Figure 5d shows the LSMO/LFO(111) interface in the epilayer for comparison. For clarity the EELS intensities have been normalized to 100% at each side (see supplementary information for non-normalized data). As can be seen, neither interface is compositionally abrupt towards the STO substrate. The signal for the substrate A-cation, Sr, decreases before the B-cation signal, Ti. Correspondingly, the A-cation signal from the thin films, La, increases before the B-cation signals, Fe/Mn respectively. The distance between the change in A and B-cation signals is determined to be 0.25 - 0.3 nm, corresponding to the distance between two subsequent A-cation layers in the (111)-orientation. The spatial resolution of the EELS signal is determined to be 0.15 nm by the width of fitted Gaussian curves for the atomically resolved EELS map. Hence, the EELS measurements reveal that the layer at the interface between film and substrate is a mixture of cations, with B-cations from the substrate and A-cations from the film. Interestingly, interfaces between subsequent epitaxial interfaces grown on (111)-oriented substrates do not have this distance between A and B-cation signals (figure 5d), hence this interface is more chemically abrupt.



Taken together, the EELS measurements reveal that the BHF substrate surfaces are Ti-rich, consistent with a surface reconstruction consisting of 1-2 TiO_x layers to screen the polarity. Figure 6a shows a model of a Sr-deficient $\text{STO}(111)$ surface with Ti-termination, where transparent blue circles at Sr positions depict Sr-vacancies in the top two Sr-layers. The non-stoichiometric surface affects the stoichiometry of the initially grown materials on the substrate and in figure 6b we display a model interface between a LFO thin film and the Sr-deficient $\text{STO}(111)$ surface. As can be seen, La now fills the position of the Sr-vacancies, effectively making a one d_{111} thick distinct $(\text{La,Sr})\text{TiO}_3$ perovskite layer, as confirmed by EELS (figure 5 b and c). The presence of an intermixed layer is in agreement with the RHEED data for the different systems investigated. The shorter period for the first RHEED oscillation indicate that less material is needed to fill the first layer. We note that the exact Sr surface composition will decide the period of the first oscillation, which therefore can vary from substrate to substrate. The model only takes into account crystalline atoms; hence, we do not include the potentially observed atomic surface Sr at the STO surface. We note that in this model the first B-cation layer in the film is stoichiometric with respect to the A/B ratio. This model is in accordance with reports on surface reconstructions in (111), where density

functional theory and experiments show that surface TiO_x layers compensate for the polarity.³²⁻³³



In conclusion, we have shown that the polar (111)-oriented STO surface can be pretreated to form single terminated, atomically smooth surfaces with both deionized water and buffered hydrogen fluoride, which promotes structurally abrupt interfaces and layer-by-layer film growth. However, the chemical interface between film and substrate is not abrupt, and one layer of chemical A-cation intermixing is found. We note that the effect is due to the substrate, and robust to the type perovskite thin film deposited. If the exact level of Sr surface vacancies can be controlled, the one interatomic thick $(\text{A},\text{A}')\text{BO}_3$ interface layer could be utilized to establish particular interface properties.

Supporting information

See supporting information for more information on CAICISS analysis and non-normalized EELS data.

Acknowledgements

This project was partially supported by the Norwegian Research Council under project number 221860 and 231290, and by JSPS Grants-in-Aid for Scientific Research Nos.

25706022 and 26105002. MN is supported by the project NORTEM (Grant 197405) within the programme INFRASTRUCTURE of the Research Council of Norway (RCN). NORTEM was co-funded by the RCN and the project partners NTNU, UiO and SINTEF.

References

1. Sanchez, F.; Ocal, C.; Fontcuberta, J., Tailored surfaces of perovskite oxide substrates for conducted growth of thin films. *Chem. Soc. Rev.* 2014, *43* (7), 2272-2285.
2. Zubko, P.; Gariglio, S.; Gabay, M.; Ghosez, P.; Triscone, J.-M., Interface Physics in Complex Oxide Heterostructures. *Ann. Rev. Cond. Mat. Phys.* 2011, *2*, 141-165.
3. Nakagawa, N.; Hwang, H. Y.; Müller, D. A., Why some interfaces cannot be sharp. *Nat Mater* 2006, *5* (3), 204-209.
4. Kawasaki, M.; Takahashi, K.; Maeda, T.; Tsuchiya, R.; Shinohara, M.; Ishiyama, O.; Yonezawa, T.; Yoshimoto, M.; Koinuma, H., Atomic Control of the SrTiO₃ Crystal Surface. *Science* 1994, *266* (5190), 1540-2.
5. Lippmaa, M.; Takahashi, K.; Ohtomo, A.; Ohashi, S.; Ohnishi, T.; Nakagawa, N.; Sato, T.; Iwatsuki, M.; Koinuma, H.; Kawasaki, M., Atom technology for Josephson tunnel junctions: SrTiO₃ substrate surface. *Mater. Sci. Eng.,B* 1998, *56* (2-3), 111-116.
6. Koster, G.; Kropman, B. L.; Rijnders, G.; Blank, D. H. A.; Rogalla, H., Quasi-ideal strontium titanate crystal surfaces through formation of strontium hydroxide. *Appl. Phys. Lett.* 1998, *73* (20), 2920-2922.
7. Blok, J. L.; Wan, X.; Koster, G.; Blank, D. H. A.; Rijnders, G., Epitaxial oxide growth on polar (111) surfaces. *Appl. Phys. Lett.* 2011, *99* (15), 151917.

8. Tasker, P. W., The stability of ionic crystal surfaces. *Journal of Physics C: Solid State Physics* 1979, 12 (22), 4977.
9. Lee, M. K.; Eom, C. B.; Tian, W.; Pan, X. Q.; Smoak, M. C.; Tsui, F.; Krajewski, J. J., Synthesis and properties of epitaxial thin films of c-axis oriented metastable four-layered hexagonal BaRuO₃. *Appl. Phys. Lett.* 2000, 77 (3), 364-366.
10. Rubi, D.; Vlooswijk, A. H. G.; Noheda, B., Growth of flat SrRuO₃ (111) thin films suitable as bottom electrodes in heterostructures. *Thin solid films* 517, 1904-1907.
11. Chakraverty, S.; Ohtomo, A.; Okude, M.; Ueno, K.; Kawasaki, M., Epitaxial Structure of (001)- and (111)-Oriented Perovskite Ferrate Films Grown by Pulsed-Laser Deposition. *Crystal Growth & Design* 2010, 10 (4), 1725-1729.
12. Hallsteinsen, I.; Boschker, J. E.; Nord, M.; Lee, S.; Rzechowski, M.; Vullum, P. E.; Grepstad, J. K.; Holmestad, R.; Eom, C. B.; Tybell, T., Surface stability of epitaxial La_{0.7}Sr_{0.3}MnO₃ thin films on (111)-oriented SrTiO₃. *J. Appl. Phys.* 2013, 113 (18), 183512.
13. Middey, S.; Rivero, P.; Meyers, D.; Kareev, M.; Liu, X.; Cao, Y.; Freeland, J. W.; Barraza-Lopez, S.; Chakhalian, J., Polarity compensation in ultra-thin films of complex oxides: The case of a perovskite nickelate. *Sci. Rep.* 2014, 4, 6819.
14. Tybell, T.; Eom, C. B., Synthesis of epitaxial multiferroic oxide thin films. In *Multifunctional Oxide Heterostructures*, Tsymbal, E. Y.; Dagotto, E. R. A.; Eom, C.-B.; Ramesh, R., Eds. Oxford University Press. : 2012.
15. Tanaka, H.; Kawai, T., Surface structure of reduced SrTiO₃ (111) observed by scanning tunneling microscopy. *Surf. Sci.* 1996, 365, 437-442.

16. Liu, Z. Q.; Lü, W. M.; Lim, S. L.; Qiu, X. P.; Bao, N. N.; Motapothula, M.; Yi, J. B.; Yang, M.; Dhar, S.; Venkatesan, T.; Ariando, Reversible room-temperature ferromagnetism in Nb-doped SrTiO single crystals. *Phys. Rev. B* 2013, *87* (22), 220405.
17. Doan, T.-D.; Giocondi, J. L.; Rohrer, G. S.; Salvado, P. A., Surface engineering along the close-packed direction of SrTiO₃. *J. Cryst. Growth* 2001, *225*, 178-182.
18. Chang, J.; Park, Y.-S.; Kima, S.-K., Atomically flat single-terminated SrTiO₃(111) surface. *Appl. Phys. Lett.* 2008, *92* (152910).
19. Biswas, A.; Rossen, P. B.; Yang, C.-H.; Siemons, W.; Jung, M.-H.; Yang, I. K.; Ramesh, R.; Jeong, Y. H., Universal Ti-rich termination of atomically flat SrTiO₃ (001), (110), and (111) surfaces. *Appl. Phys. Lett.* 2011, *98* (5), 051904.
20. Connell, J. G.; Isaac, B. J.; Ekanayake, G. B.; Strachan, D. R.; Seo, S. S. A., Preparation of atomically flat SrTiO₃ surfaces using a deionized-water leaching and thermal annealing procedure. *Appl. Phys. Lett.* 2012, *101* (25), 251607.
21. Peña, F. d. l.; Burdet, P.; Ostasevicius, T.; Sarahan, M.; Nord, M.; Fauske, V. T.; Taillon, J.; Eljarrat, A.; Mazzucco, S.; Donval, G.; Zagonel, L. F.; Walls, M. *hyperspy: HyperSpy 0.8.2*.
22. Iwahori, K.; Watanabe, S.; Komeda, T.; Kawai, M.; Saito, A.; Kuwahara, Y.; Aono, M., Force Microscopy Study of SrTiO₃ (001) Surfaces with Single Atomic-Layer Steps. *Jpn. J. Appl. Phys.* 1999, *38* (6S), 3946.
23. Ohnishi, T.; Shibuya, K.; Lippmaa, M.; Kobayashi, D.; Kumigashira, H.; Oshima, M.; Koinuma, H., Preparation of thermally stable TiO₂-terminated SrTiO₃(100) substrate surfaces. *Appl. Phys. Lett.* 2004, *85* (2), 272-274.

24. Russell, B. C.; Castell, M. R., Surface of Sputtered and Annealed Polar SrTiO₃(111): TiO_x-Rich (n × n) Reconstructions. *J. Phys. Chem. C* 2008, *112*, 6538-6545.
25. Chiamonti, A. N.; Lanier, C. H.; Marks, L. D.; Stair, P. C., Time, temperature, and oxygen partial pressure-dependent surface reconstructions on SrTiO₃(1 1 1): A systematic study of oxygen-rich conditions. *Surf. Sci.* 2008, *602* (18), 3018-3025.
26. Haruyama, Y.; Aiura, Y.; Bando, H.; Nishihara, Y.; Kato, H., Annealing temperature dependence on the electronic structure of the reduced SrTiO₃ (111) surface. *J. Electron Spectrosc. Relat. Phenom.* 1998, *88-91*, 695-699.
27. Tanaka, H.; Kawai, T., Surface structure of reduced SrTiO₃(111) observed by scanning tunneling microscopy. *Surf. Sci.* 1996, *365* (2), 437-442.
28. Yin, Y.; Wang, J.; Zhu, H.; Lv, K.; Wu, X. S., Structural distortion and charge redistribution in SrTiO₃ (111) polar surfaces. *Vacuum* 2015, *120, Part A*, 83-88.
29. Sullivan, M. C.; Ward, M. J.; Gutiérrez-Llorente, A.; Adler, E. R.; Joress, H.; Woll, A.; Brock, J. D., Complex oxide growth using simultaneous in situ reflection high-energy electron diffraction and x-ray reflectivity: When is one layer complete? *Appl. Phys. Lett.* 2015, *106* (3), 031604.
30. Rijnders, G.; Blank, D. H. A.; Choi, J.; Eom, C.-B., Enhanced surface diffusion through termination conversion during epitaxial SrRuO₃ growth. *Appl. Phys. Lett.* 2004, *84* (4), 505-507.
31. Chang, J.; Park, Y.-S.; Lee, J.-W.; Kim, S.-K., Layer-by-layer growth and growth-mode transition of SrRuO₃ thin films on atomically flat single-terminated SrTiO₃ (111) surfaces. *J. Cryst. Growth* 2009, *311*, 3771-3774.

32. Herger, R.; Willmott, P. R.; Bunk, O.; Schlepütz, C. M.; Patterson, B. D.; Delley, B.; Shneerson, V. L.; Lyman, P. F.; Saldin, D. K., Surface structure of SrTiO₃(001). *Phys. Rev. B* 2007, 76 (19), 195435.
33. Marks, L. D.; Chiaramonti, A. N.; Rahman, S. U.; Castell, M. R., Transition from Order to Configurational Disorder for Surface Reconstructions on SrTiO₃(111). *Phys. Rev. Lett.* 2015, 114 (22), 226101.

Figure captions

Figure 1: Schematic of an ideal cubic STO (111) Ti^{4+} terminated surface, with Ti in yellow, Sr in blue and O in turquoise. The Ti^{4+} layers are indicated by dashed lines, and labeled A,B,C according to the “ABCABC...” stacking. a) Cross-section view. The distance between two equivalent lattice planes is $d_{111} = a/\sqrt{3} = 2.25 \text{ \AA}$, where a is the cubic lattice constant of SrTiO_3 ($a = 3.905 \text{ \AA}$) b) top view. Arrows indicate the low-index in-plane crystallographic directions $[10\bar{1}]$ and $[11\bar{2}]$.

Figure 2: AFM images (tapping mode) of STO(111) surfaces with different pretreatments a) As-received, b) BHF, c) DI d) Line profiles between points A and B extracted from b) and c). AFM images (tapping mode) of LSMO thin films (10nm thick) grown on e) As-received, f) BHF g) DI treated substrates. All images areas are $3 \times 3 \mu\text{m}^2$.

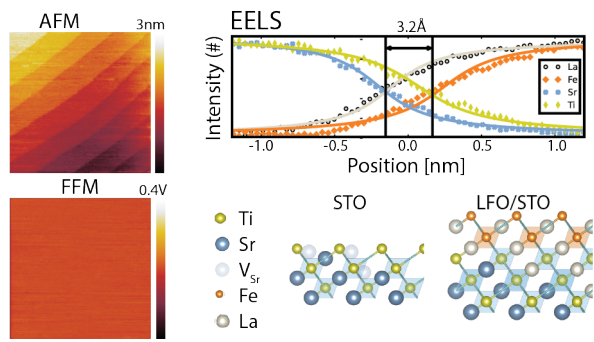
Figure 3: Contact mode AFM and FFM of STO(111) with different pretreatments: a,b) BHF method, c,d) DI method, and e,f) The DI sample after an additional water rinse. The AFM and FFM images were acquired simultaneously, the image area is $3 \times 3 \mu\text{m}^2$.

Figure 4: a) RHEED intensity profiles for initial growth of LSMO, LFO and BTO films on top of $\text{SrTiO}_3(111)$ pretreated by BHF. The profiles are normalized to growth period. The first oscillation of all three examples has a shorter period than the rest. b) Statistics of the period for the RHEED intensity profiles for initial growth of LSMO and LFO. The growth period is plotted against $\log(\text{RHEED oscillations})$ for clarity c) RHEED intensity profile for a complete bilayer; LSMO/LFO/ $\text{SrTiO}_3(111)$. The first oscillation for the second layer has the same growth period as the rest of the oscillations.

Figure 5: STEM-EELS characterization of film interfaces. a) STEM-HAADF image of LSMO/STO(111) interface and EELS chemical line scans of b) LSMO/STO(111), c) LFO/STO(111), and d) LSMO/LFO(111) interfaces. The EELS line scans has been normalized to 100% at each side of the interface.

Figure 6: Model of (111)-oriented STO/film interface a) Substrate surface with Sr-deficient top layers and b) interface with LFO, where La-atoms has filled in the Sr-vacancies, yielding a (La,Sr)TiO₃ layer at the interface. Atoms are colored accordingly; Ti atoms are yellow, Sr blue, Sr vacancies transparent blue, La gray, Fe orange. Oxygens are shown as octahedral.

For tables of contents use only



Substrate surface preparation of polar SrTiO₃(111) reveals smooth step-and-terrace surfaces with single termination. Subsequent film growth reveals that the interface consist of a single chemically intermixed (A,A')BO₃ perovskite layer, which we interpret to be A'-cations from the film filling in A-vacancies at the surface. A surface reconstruction of the substrate consisting of TiO_x layers is consistent with such a picture.

